Light-Writing and Projecting Multicolor Fluorescent Hydrogels for On-Demand Information Display

Shuxin Wei, Wei Lu,* Huihui Shi, Shuangshuang Wu, Xiaoxia Le, Guangqiang Yin, Qingquan Liu, and Tao Chen*

Intelligent rewritable display systems have been long expected to reduce the heavy consumption of single-use or transient devices in the age of Internet-of-Things. However, it remains challenging to construct such systems with integrated functionality of remote control, rapid activation, multicolor and multimode display. Herein, by learning from the unique multilayer arrangement of chromatophores in chameleon skins, a promising kind of rewritable hydrogel multicolor systems is presented that can combine the merits of near-infrared (NIR) light-writing and projecting modes for on-demand information display. Specifically, the systems have typical multilayer layout consisting of poly(dimethylsiloxane) (PDMS)-sealed carbon nanotubes (CNTs) film as photothermal control unit and embedded fluorescent hydrogels as multicolor display unit, in which thermoresponsive hydrogel is constrained within non-responsive hydrogel. Such rational structure design results in the establishment of one promising display mechanism via the cascading "light trigger–heat generation–fluorescence output" process. On this basis, rapid and reversible hand-written display of arbitrary information is achieved within 5 s. Also, sustainable light-projecting display of predesigned multicolor patterns is demonstrated due to the multilayer design that ensures easy patterning of photothermal control or hydrogel display layer. This study brings functional-integrated merits for novel rewritable display systems and open new possibility to construct high-end products for information display/transmission.

1. Introduction

In the age of the Internet-of-Things, intelligent rewritable display materials can be promising candidates to solve the growing electronic waste and potential ecological pollution caused by heavy consumption of single-use or transient systems.[1] They are thus expected to become the next-generation medium for information display and transmission. So far, a number of rewritable display systems have been reported, which enabled the reversible writing of certain information (e.g., text, patterns, and figures) and subsequent erasure to facilitate another information writing cycle.[2] However, since most reported systems were chemically responsive, information writing/erasing/rewriting of these materials were primarily achieved by the alternating usage of different chemicals (e.g., water, ions, acid/base, or urea solution). These systems easily suffered from chemical product residue/accumulation caused by the alternating usage of chemical inks that would largely reduce the rewritability and reversible display sensitivity.

The residue-free light-writing display with remote, local, and precise controllability is believed to be an attractive strategy to address these difficult challenges. Also, the wavelength and intensity of light can be modulated in time and space without physical contact.[3] On the basis of this consensus, a number of elegant light-writing display systems have been reported over the past decade, in which the achievement of writing/erasing/rewriting relied on the light-triggered covalent chemical structure transformations of certain molecules,[4] including *cis–trans* isomerism of azobenzene derivatives,[5] ring-opening reaction of spiropyrane.[6] Nevertheless, this classic strategy is often limited to a few types of delicately synthesized molecules (azobenzene, spiropyrane, etc.) with relatively slow light-response kinetics (≈tens of seconds). To trigger these photochemical covalent reactions, high-energy UV or short-wavelength visible light are needed. Moreover, reversible efficiency of photochemical reaction is usually not 100%. These problems make it quite challenging to satisfy the need for fast and sustainable writing/erasing/rewriting display. To conquer these limitations, one promising idea is to utilize the low-energy

S. Wei, W. Lu, H. Shi, S. Wu, X. Le, G. Yin, T. Chen
Key Laboratory of Marine Materials and Related Technologies
Zhejiang Key Laboratory of Marine Materials and Protective Technologies
Ningbo Institute of Materials Technology and Engineering
Chinese Academy of Sciences
Ningbo 315201, China
E-mail: luwei@nimte.ac.cn; tao.chen@nimte.ac.cn
S. Wei, W. Lu, H. Shi, S. Wu, X. Le, G. Yin, T. Chen
School of Chemical Sciences
University of Chinese Academy of Sciences
Beijing100049, China
Q. Liu
Hunan Provincial Key Laboratory of Advanced Materials for New Energy Storage and Conversion
Hunan University of Science and Technology
Xiangtan 411201, China

but high-penetrating near-infrared (NIR) light[7] as the "writing pen" to generate local photo-heat that will trigger the fast and reversible responses of supramolecular chromophore assemblies. For example, fast NIR light-writing/self-erasing/rewriting display of transient information (e.g., Arabic numbers, English letters) was creatively achieved in thermo-responsive poly(*N*-isopropyl acrylamide) (PNIPAM) gel by utilizing the "light+heat" of co-existing liquid metal nanoparticles to regulate the polarity-related fluorescent intensity of rhodamine B.[8] However, the resultant system failed to achieve the sustainable display of predesigned patterns because of its homogeneous structure that greatly raised the difficulty of material patterning. Also, colorful fluorescent patterns/information could not be displayed owing to its simple switching behavior of single-color fluorescence. There is thus a great interest to develop new-concept NIR light-responsive systems, which utilize the low-energy and highly controllable NIR light to generate local photo-heat to trigger the instant and reversible fluorescence color changes of thermo-responsive supramolecular chromophore assemblies. Such systems are envisaged to enable not only the fast, reversible, and multicolor light-writing display of transient information, but also the sustainable light-projecting display of predesigned colorful patterns. Such functional integrated display capability helps to meet the differential display/transmission requirements for various kinds of information, and also better visual information interactive experience.

Astonishingly, it is a wonder that these integrated display advantages could be combined in the soft skins of natural chameleons. As masters of color change, chameleons can exhibit diverse skin colors and patterns for better adaption to dynamic living environments. Biological and anatomical studies revealed that such wonderful multicolor pattern display characteristics of chameleon skins are derived from their vertical arrangement of multilayered chromatophores (xanthophores, iridophores, and melanophores, **Figure 1**A).[9] Upon external stimuli, differential aggregation/dispersion behaviors of pigment granules within each skin chromatophore layer instantly arise to vary their color-mixing proportions, resulting in diverse skin colors. Such vertical multilayer structure and efficient synergy of each functional layer thus constitute the evolutionary novelty of chameleons that allow their soft skins to exhibit rapid, reversible, and sustainable display of diverse colorful patterns. Inspired by this finding, we propose that if NIR photothermal materials and temperature-responsive color-changing materials were rationally arranged according to such evolution-optimized multilayer structure design, it would be promising to produce conceptually new rewritable systems that enabled rapid, sustainable, and multicolor writing/self-erasing/rewriting for on-demand information display.

To demonstrate this hypothesis, a proof-of-concept material design was reported herein based on life-like fluorescent polymeric hydrogel that possesses similar soft wet nature and mechanical strength to natural chameleon skins,[10] as well as thermo-responsive color changes. The developed rewritable display system consists of vertically arranged fluorescent polymeric hydrogel layer as the multicolor display unit, and poly(dimethylsiloxane) (PDMS)-sealed stacked carbon nanotubes (CNTs) film layer as the photothermal control unit (Figure 1B). To ensure the intact, reversible, and multicolor

writing/self-erasing behaviors, the hydrogel display layer was specially designed with an embedded multilayer structure, in which the PNIPAM-based temperature-responsive Eu^{3+}-coordinated red fluorescent inner-core hydrogel was stably constrained in the non-responsive blue fluorescent outer-shell hydrogel. As illustrated in Figure 1B,C; Figure S1 (Supporting Information), when NIR laser served as a non-contact "pen" for remote writing, photo-heat would be locally generated by the CNTs thin film layer and transferred to elevate the temperature of PNIPAM-based fluorescent hydrogel to above its volume phase transition temperature (VPTT, ≈34 °C), leading to the formation of hydrogen-bonded (–C≡O···H–N–) dynamic crosslinks and hydrophilic-hydrophobic phase transition of the inner-core hydrogel. As a result, the polymer network was largely shrunken to significantly reduce the water solvation effect of Eu^{3+}-coordinated luminogens and thus enhance red fluorescence of the inner-core hydrogel to achieve the instant light-writing display (≈5 s). Owing to the constraining effect of non-responsive outer-shell hydrogel in this specially designed embedded structure, the temperature-responsive inner-core hydrogel can maintain shape and position stability in the photothermal writing process. When NIR laser was off, temperature of the irradiated area would spontaneously drop to room temperature (RT), bringing PNIPAM-based hydrogel back to the hydrophilic state with fluorescence intensity recovery to allow the rewriting of other information. More importantly, such bio-inspired multilayer layout has been demonstrated to facilitate easy patterning of either the photothermal CNTs layer or the fluorescent hydrogel display layer. Consequently, the sustainable light-projecting display of well-defined multicolor patterns could be maintained under the input of area NIR light source. Such NIR light-responsive display systems, which combined the integrated capacity to enable both fast light-writing/erasing/rewriting of transient information and sustainable light-projecting of predesigned multicolor patterns, are expected to open new possibility to construct sustainable high-end products for information display and transmission.

2. Results and Discussion

2.1. Design and Fabrication of the Fluorescent Hydrogel Layer with Embedded Structure as the Display Unit

Key design of the photothermally controlled rewritable system was the fluorescent hydrogel layer with an embedded structure, which served as display unit. It was constructed by two-step thermally initiated radical polymerization (**Figure 2**A,B; Figure S2, Supporting Information). The inner-core hydrogel with temperature-induced tunable fluorescent properties was fabricated in the 1st polymerization. Next, the precursor solution of outer-shell hydrogel was added around the preformed inner-core hydrogel in a larger mold, followed by the 2nd thermally initiated radical polymerization. After that the inner-core hydrogel was stably embedded in the outer-shell hydrogel through interfacial polymer network interpenetration and physical crosslinking. Specifically, the inner-core hydrogel was synthesized by thermally initiated radical polymerization of a specially designed chelating ligand potassium 6-acrylamidopicolinate (K6APA), NIPAM, methylene bisacrylamide, and nanoclay. Then the as-prepared PNIPAM-K6APA hydrogel was immersed in Eu^{3+}
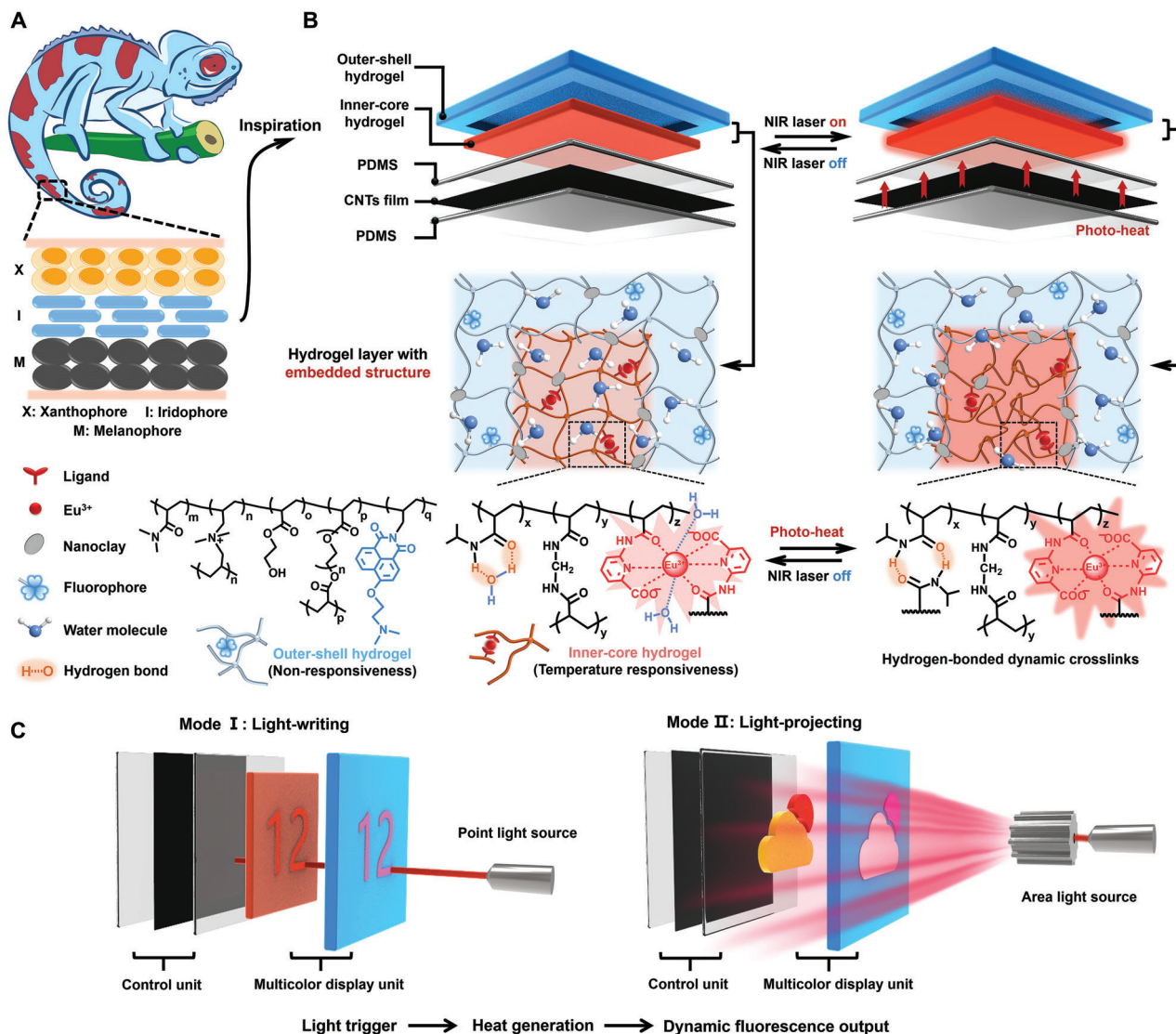
Figure 1. Design of the rewritable hydrogel display system with biomimetic vertical multilayer structure. A) Schematic illustration showing the arrangement of several types of chromatophores (xanthophore, iridophore, and melanophore) in chameleon skin with a vertical multilayer structure. B) Illustration of the rewritable hydrogel display system consisting of PDMS-sealed stacked CNTs film as NIR photothermal control unit and embedded fluorescent hydrogels as multicolor display unit, in which thermo-responsive inner-core hydrogel is constrained within non-responsive outer-shell hydrogel. Photo-heat generated by the CNTs thin film layer would lead to the formation of hydrogen-bonded (−C≐O···H−N−) dynamic crosslinks and hydrophilic-hydrophobic phase transition of the inner-core hydrogel. As a result, the polymer network was largely shrunken to significantly reduce the water solvation effect of Eu^{3+}-coordinated luminogens and thus enhance red fluorescence of the inner-core hydrogel. C) Schemes illustrating the fast, reversible, and multicolor light-writing display of transient information, and the sustainable light-projecting display of colorful patterns through the cascading mechanism of "light trigger–heat generation–dynamic fluorescence output".

aqueous solution to fabricate Eu-PNIPAM hydrogel, which was highly transparent under daylight but red fluorescent under 254 nm UV light (Figure S3, Supporting Information). The formation of lanthanide complexes in the obtained Eu-PNIPAM hydrogel was characterized by Fourier transform infrared (FT-IR) and X-ray photoelectron spectroscopy (XPS) (Figure S4–5, Supporting Information). Notably, PNIPAM-based hydrogels are known to exhibit a distinct and reversible thermo-responsive behavior below and above their VPTT.[11] The hydrophilic–hydrophobic phase transition can be well controlled by the temperature. As re-

vealed by SEM images in Figure 2C, the Eu-PNIPAM hydrogels had large honeycomb-shaped porous crosslinked network at RT, indicating their highly water-swollen state. With increasing temperature to above the VPTT (e.g., 60 °C), the polymer network was largely collapsed to show small porous crosslinked network, suggesting the formation of hydrogen-bonded (−C≐O···H−N−) dynamic crosslinks in the hydrogels. To gain insight into the detailed functional group changes of PNIPAM chains in the hydrophilic–hydrophobic phase transition process, variable-temperature FT-IR spectroscopy was conducted (Figure 2D). Upon raising temperature from
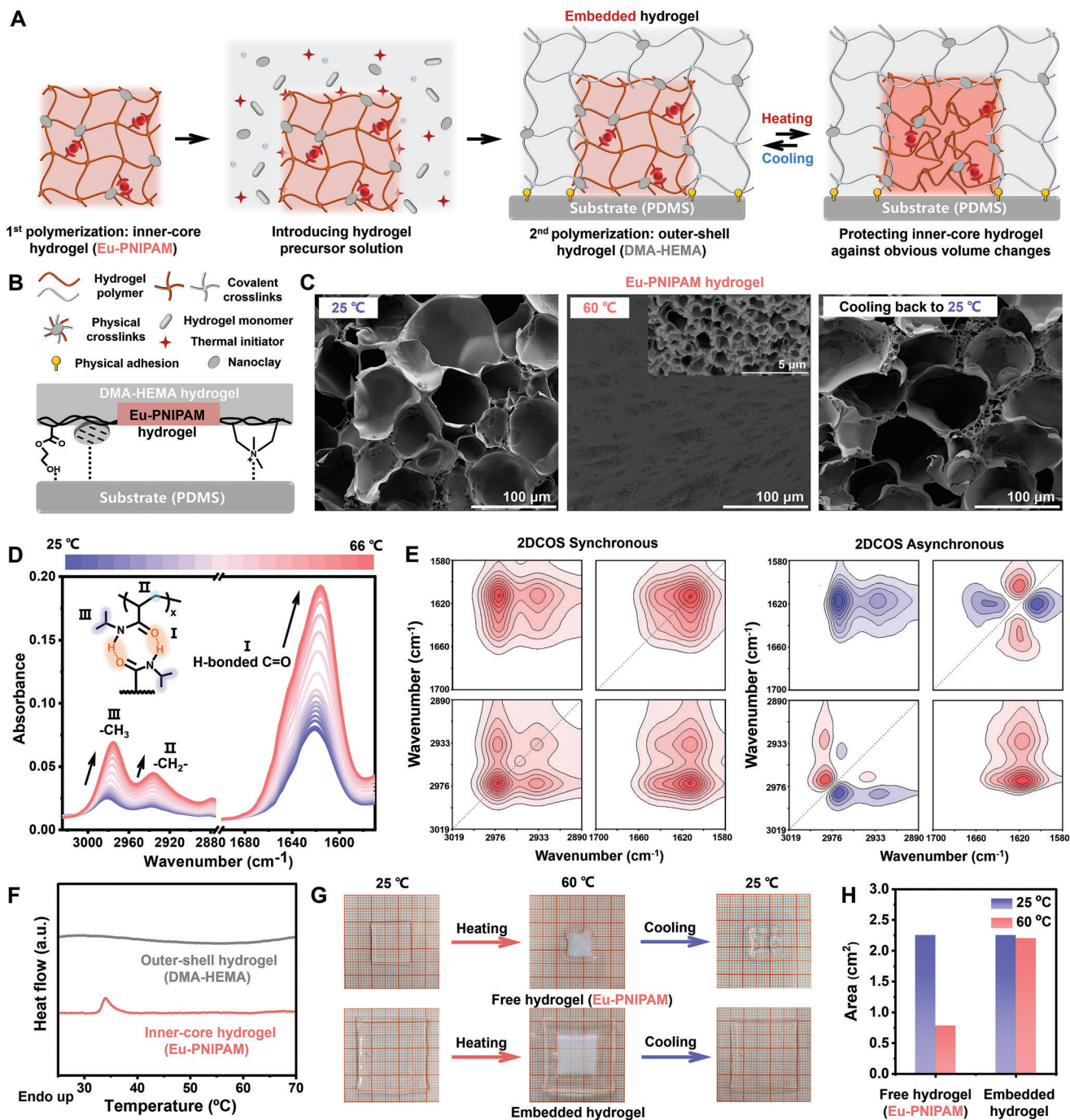
Figure 2. Fabrication and characterization of the hydrogel display layer. A) Illustration of the two-step polymerization of the embedded hydrogel and its thermally triggered phase transition mechanism. B) Schematic of the intermolecular interactions between the DMA-HEMA hydrogel and the PDMS substrate. C) SEM images of Eu-PNIPAM hydrogels at 25 °C, 60 °C, and after cooling back to 25 °C. D) Temperature-dependent FT-IR spectra of PNIPAM hydrogel upon heating from 25 to 66 °C (The solution is D_2O), and E) corresponding 2D correlation spectroscopy (2DCOS) synchronous and asynchronous spectra, in which red and blue colors represent positive and negative intensity, respectively. F) DSC curve of inner-core and outer-shell hydrogels. G) Photographs showing shape changes of the free Eu-PNIPAM hydrogel and embedded hydrogel triggered by adjusting the temperature from 25 °C to 60 °C and returning to 25 °C, as well as H) the corresponding area size changes of these two samples. Scale bar: 1 cm.

**ADVANCED
SCIENCE NEWS**

www.advancedsciencenews.com

**ADVANCED
MATERIALS**

www.advmat.de

25 °C to 66 °C, the C≐O stretching band centered at 1622 cm^{-1} shifted to lower wavenumbers (1616 cm^{-1}) accompanying with enhanced intensity, which provided direct evidence for the formation of hydrogen-bonded (–C≐O···H–N–) dynamic crosslinks. The peaks of CH$_3$ stretching band of the side chains of PNIPAM, and CH$_2$ stretching band of the main chains both performed red shift from 2981 cm^{-1} to 2975 cm^{-1}, and from 2938 cm^{-1} to 2936 cm^{-1}, respectively, demonstrating the dehydration of the CH$_3$ and CH$_2$ groups.[12] 2D correlation spectroscopy (2DCOS) analysis was further conducted to show microdynamics mechanism of this PNIPAM system in the heating process (Figure 2E). The synchronous 2D-IR spectrum in the 3019–2890 cm^{-1} range was dominated by two strong autopeaks at 2975 and 2936 cm^{-1}, while in the 1700–1580 cm^{-1} range was dominated by one strong autopeak at 1616 cm^{-1}. The symbol of the cross-peak at (1616, 2975 cm^{-1}) and (2975, 2936 cm^{-1}) were positive in the synchronous and asynchronous maps. Therefore, the event sequence was 1616 > 2975 > 2936 cm^{-1}, indicating that intramolecular hydrogen bonds were formed first, followed by enhanced hydrophobic associations of the isopropyl groups through dehydration, and finally the collapse and aggregation of the polymer main chains in the temperature-induced phase transition process. These results have clearly demonstrated the thermoresponsive chemical mechanism of the display unit.

The outer-shell hydrogel was synthesized by radical polymerization of N,N-dimethylacrylamide (DMA) and 2-hydroxyethyl methacrylate (HEMA), as well as diallyldimethylammonium chloride (DADMAC), poly(ethylene glycol) diacrylate (PEGDA) and nanoclay as crosslinkers. It was briefly named as DMA-HEMA hydrogel. Owing to its unique multiply crosslinked networks, the optimized DMA-HEMA hydrogel was proved to have excellent mechanical properties (Figure S6, Supporting Information). Also, the presence of high-density functional groups like –OH and plenty of negative charges from nanoclay and positive charges from DADMAC helped the embedded hydrogel stably adhere to the PDMS substance through hydrogen bonding, electrostatic and dipole interactions (Figure 2B; Figure S7, Supporting Information). The lap shear adhesion test indicated that the DMA-HEMA hydrogel had good adhesive capacity to PDMS film with the adhesion strength of 104.6 KPa (Figure S8, Supporting Information).

Besides ensuring stable adhesion with the PDMS substrate, the embedded structure also promised to keep the size stability of hydrogel display unit during the photothermal writing processes. As described above, the inner-core Eu-PNIPAM and outer-shell DMA-HEMA hydrogels were specially designed into the embedded structure and strongly bonded together by interfacial polymer network interpenetration, and the polymer chains entanglement around the nanoclay (Figure S9, Supporting Information). As shown in Figure S10 (Supporting Information), such interfacial bonding strength was even greater than the bulk strength of Eu-PNIPAM hydrogel, as evidenced by the tensile experiment which showed the tensile fracture occurred at the hydrogel ontology rather than the joint. Further DSC illustrated the outer DMA-HEMA hydrogel had almost no thermodynamic change in the range of 25 °C to 70 °C, while the inner-core Eu-PNIPAM hydrogel had obvious phase transition with a VPTT of ≈34 °C (Figure 2F). The variable temperature rheology measurement also proves the result (Figure S11, Supporting Information).

As expected, large size shrinkage (≈65%) was observed for the free Eu-PNIPAM hydrogel upon temperature elevation to 60 °C (Figure 2G,H). And its morphology curled severely in the cooling process. However, it was astonishingly found that the area of inner-core Eu-PNIPAM hydrogel constrained in the embedded structure was nearly unchanged following the same heating-induced phase transition. Also, the morphology of the embedded hydrogel still maintained flatness, which could be clearly observed in the side view (Figure S12, Supporting Information). This could provide an excellent platform for subsequent dynamic information loading. Such excellent size and morphology stability was derived from the embedded structure design of our hydrogel display unit, in which the strong interfacial bonding between two hydrogel layers helped the inner-core Eu-PNIPAM hydrogel against the shrinking force brought by the heat-induced phase transition.

2.2. Rational Arrangement of the Embedded Hydrogel and PDMS-Sealed Photothermal CNTs Film into Bio-Inspired Multilayer Structure

To promote the triggering stimulus for phase transition of the embedded hydrogel display layer from heat to NIR light, the photothermal layer needs to be introduced to form bio-inspired multilayered structure. To this end, the condensed CNTs film was first fabricated at the air/water interface according to the previously reported method.[13] Subsequently, commercial PDMS film (0.5 mm thickness) was used to transfer the CNTs film to produce the bilayer CNTs/ PDMS film. As observed from SEM images (Figure S13, Supporting Information), its CNTs side showed inter-stacked tubular CNTs network, while its PDMS side exhibited smooth surface. To ensure the long-term stability of photothermal layer, PDMS precursor solution was then added and cured on the CNTs side to form the PDMS/CNTs/PDMS film (1.0 mm thick) with sandwiched structure (**Figure 3**A; Figure S14, Supporting Information). The encapsulated CNTs film can be effectively protected to prevent damage from external forces like finger scratching and tape sticking (Figure S15, Supporting Information). Through the above method, the PDMS/CNTs/PDMS films with different ply numbers; (x) of condensed CNTs films (x = 0–4, briefly named as PDMS/CNTs/PDMS-x) were prepared. Their photos shown in Figure 3B indicated obvious color darkening as the ply number of CNTs film increased. This observation was consistent with the UV-vis-NIR spectral results recorded in the range of 380–1200 nm (Figure 3C; Figure S16, Supporting Information). Compared with pure PDMS film, the PDMS/CNTs/PDMS-x films had lower transmission and reflection, resulting in higher absorption in the short-wavelength NIR region. Their absorption was significantly enhanced as the ply number of CNTs film increased. For the PDMS/CNTs/PDMS-3 and PDMS/CNTs/PDMS-4 samples, the absorption reached more than 79% at 808 nm, clearly revealing their high-efficiency photo-adsorption.

Then, the photothermal conversion properties of these PDMS/CNTs/PDMS-x films were systematically investigated. Under illumination with 808 nm laser (20 W cm^{-2}), the pure PDMS film as a control showed barely any temperature change, while the temperature of all PDMS/CNTs/PDMS-x

**ADVANCED
SCIENCE NEWS**

www.advancedsciencenews.com
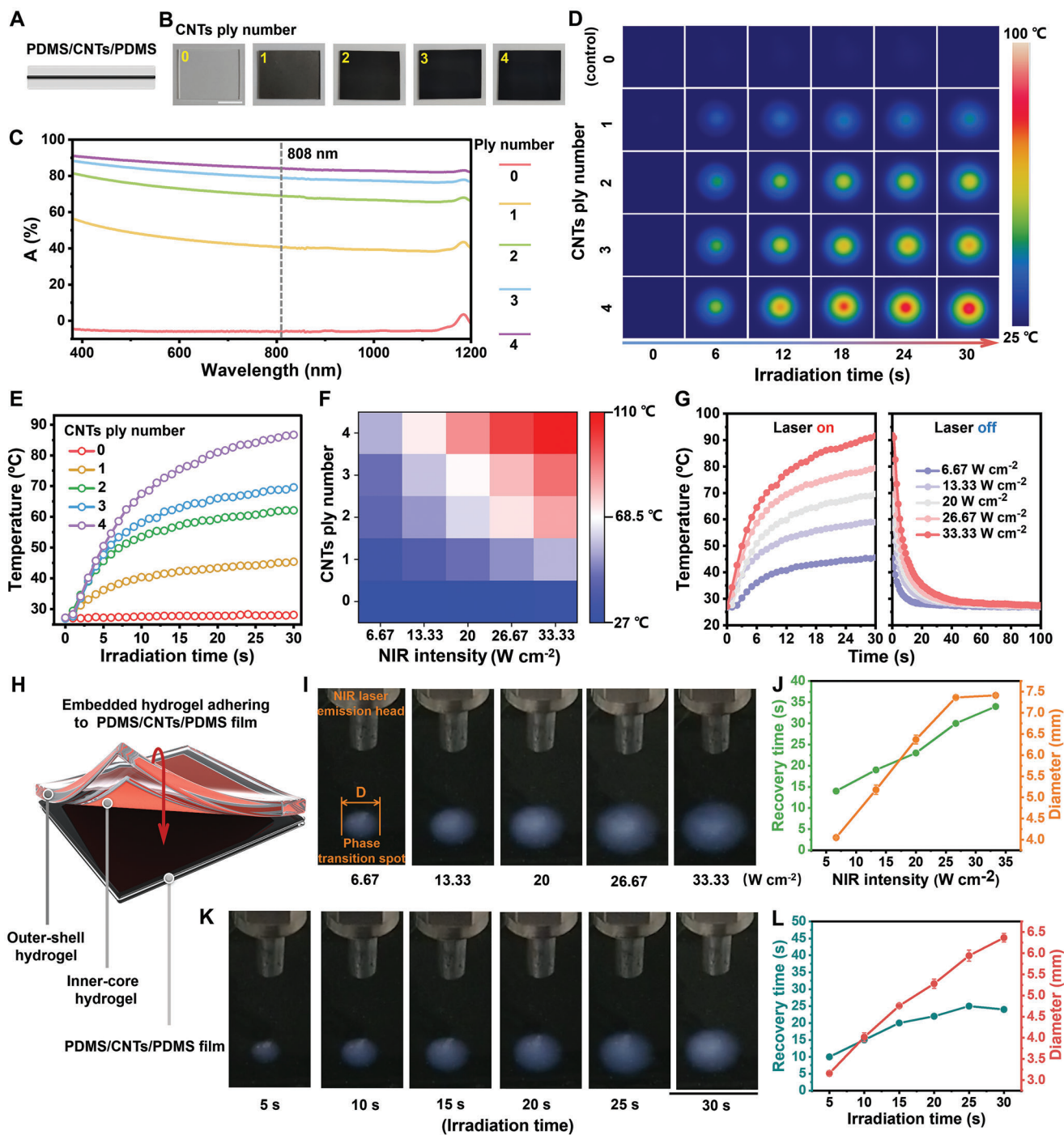
**ADVANCED
MATERIALS**

www.advmat.de

Figure 3. Photothermal performance studies. A) Schematic illustration showing the sandwiched structure of PDMS/CNTs/PDMS film. B) Digital photos of PDMS/CNTs/PDMS-*x* film with different ply numbers of condensed CNTs films (*x* = 0-4). C) UV-vis-NIR absorption spectra of PDMS/CNTs/PDMS-*x* films. D) IR images of the photothermal layers taken at different time intervals under illumination with 808 nm laser (20 W cm^{-2}). E) Temperature changes of these PDMS/CNTs/PDMS films as a function of irradiation time at 20 W cm^{-2}. F) Surface temperature of the samples with various NIR intensity. G) Time-dependent temperature profiles of the PDMS/CNTs/PDMS-3 film recorded upon power on—off of different NIR intensities. H) Construction of the rewritable hydrogel display system through combining the embedded hydrogel and PDMS/CNTs/PDMS film. I) Photographs showing phase transition spots of the hydrogel with different NIR intensities at 30 s light irradiation. J) The recovery time and the phase transition spot diameter of the hydrogel layer with increasing NIR intensity. K) Photographs showing phase transition spots of the hydrogel layer with different irradiation time at 20 W cm^{-2}. L) The recovery time and the phase transition spot diameter of the hydrogel layer with increasing irradiation time. Scale bars in digital photos are 1 cm.

**ADVANCED
SCIENCE NEWS**

www.advancedsciencenews.com

**ADVANCED
MATERIALS**

www.advmat.de

films was quickly raised with an increase in the ply number of CNTs film or irradiation time (Figure 3D,E). Among them, the PDMS/CNTs/PDMS-3 and PDMS/CNTs/PDMS-4 samples had very fast photothermal response rates, as their surface temperatures increased to more than 33 and 47 °C under the irradiation time of only 2 and 5 s, respectively. Besides, the photothermal effect was also found to be positively related to the exposed laser power density, suggesting the possibility for remote control of the generated photo-heat by facilely varying the laser power (Figure 3F). PDMS/CNTs/PDMS-3 was chosen for the following study, because the surface temperature of PDMS/CNTs/PDMS-4 could reach above 80 °C with prolonged illumination time or increased NIR intensity, which may bring damage to the whole display device. Figure 3G depicted the temperature profiles of PDMS/CNTs/PDMS-3 upon power on-off of different light intensity of NIR laser. It was found its surface temperature increased rapidly in a short time (within 5 s) to above the VPTT (34 °C) of Eu-PNIPAM hydrogel by elevating the laser power density to above 13.33 W cm^{-2}. When the laser was turned off, the temperature decreased sharply and then gradually returned to the RT within 20≈40 s. Notably, the main reason why the temperature can drop quickly is that the NIR light spot is highly focused and its diameter on the photothermal CNTs layer can be accurately controlled to be ≈2 mm. Therefore, the photo-heat concentrated in such a small area can diffuse to the surroundings spontaneously and quickly in tens of seconds.

Next, the flexible hydrogel display system was constructed by interfacially adhering the as-prepared embedded hydrogel to the optimized PDMS/CNTs/PDMS-3 film (Figure 3H; Figure S17, Supporting Information). Such layout enables in situ temperature control of the inner-core hydrogel in a remote way. Specifically, upon illumination with 808 nm laser, the generated heat of CNTs film was spontaneously transferred to the inner-core Eu-PNIPAM hydrogel, resulting in its instant phase transition. As depicted in Figure 3I–L, the size of phase transition region in the hydrogel was positively correlated with the laser power density and laser irradiation time. Notably, an obvious phase transition with the diameter of ≈3.16 mm can be clearly observed under a short time (5 s) of NIR laser irradiation at 20 W cm^{-2}. After turning off the NIR light, the phase transition region gradually recovered to the transparent state. Similarly, the recovery time also basically increased with higher NIR intensity or longer exposure time (Figure 3J,L; Figure S18–19, Supporting Information). These results suggested that the photo-heat transferred to the NIR light writing area could be facilely controlled by regulating the laser power density and laser irradiation time. Consequently, the highly controllable photothermal stimulus in terms of adjustable phase transition dimension and recovery time laid a solid foundation for on-demand light-writing of dynamic information on the flexible multilayer-structured display system.

2.3. "Light Trigger–Heat Generation–Dynamic Fluorescence Output" Cascading Process

Due to the bioinspired vertical multilayer structure of our flexible display system, one promising cascading display mechanism of "light trigger–heat generation–dynamic fluorescence output" was further achieved, enabling the remote and local control over fluorescence response of the embedded hydrogel display unit by facilely controlling the NIR laser input on the CNTs film. The inner-core Eu-PNIPAM hydrogel was red fluorescent due to the antenna effect of K6APA ligand that transferred the absorption energy to sensitize lanthanide luminescence (Figure S20–S22, Supporting Information). Notably, water solvation effect of lanthanide complexes greatly affects their luminous intensity.[14] Frequent water collisions and non-radiative decay processes containing high-energy –OH vibrations make the excited state of Eu^{3+} ions easily quench in aqueous solutions.[15] Therefore, the photoluminescence quantum yield of Eu-K6APA aqueous solution was only 1.12% (**Figure** 4A). The formation of the hydrogel network effectively reduced its water solvation effect to enhance the luminescence efficiency of Eu-PNIPAM hydrogel by 5.4 times. Furthermore, through in situ freeze drying Eu-PNIPAM hydrogel to remove all the water in the polymer network, the photoluminescence quantum yield increased rapidly to reach 19.19%. Interestingly, when heated above the VPTT, Eu-PNIPAM hydrogels underwent hydrophilic–hydrophobic phase transition, which could effectively reduce the water solvation effect of lanthanide coordination to increase red emission (Figure 4B). This finding provided the cornerstone for the desired photothermal writing technique. For achieving better display legibility, the thickness of outer-shell DMA-HEMA hydrogel was systematically optimized to minimize its influence on the fluorescence light transmittance (Figure S23, Supporting Information). As can be seen from Figure 4C; Figure S24 (Supporting Information), it was found that the embedded hydrogel with 0.3 mm thick outer-shell hydrogel exhibited bright red emission color, and thus was chosen to construct the following light-writing system.

Based on the above-established cascading display mechanism of "light trigger–heat generation–dynamic fluorescence output", real-time non-contact dynamic information display can be realized. As illustrated in Figure 4D,E, a handwritten letter "N" was clearly displayed on the hydrogel layer by using 808 nm laser as the "pen". In this process, NIR laser with high penetration could pass through the embedded hydrogel layer to reach the photothermal layer for efficient photothermal conversion. The generated heat was in turn transferred to the hydrogel layer, resulting in the local phase transition, and weakening of water solvation effect of lanthanide coordination. It further led to red fluorescence enhancement of inner-core Eu-PNIPAM hydrogel at the irradiated region. Consequently, the light-written letters could be easily recognized. When the NIR laser was turned off, temperature of the writing area dropped rapidly to make the phase-change area return to hydrophilic state, accompanying with the recovery of water solvation effect and red fluorescence intensity. As shown in Figure 4E, such NIR-light-written information could be read within ≈20 s, and will be completely self-erased after 36 s. Notably, because of the highly reversible thermosensitivity of hydrogel display unit, the prepared system exhibited excellent "writing/self-erasing/rewriting" display ability. Therefore, the letter "I" could be rewritten by using laser light, and then completely erased to allow the rewriting of the letter "R". Each letter was legible and self-erasable. Similarly, more information like "UCAS", "1978", and Arabic numbers (0–9) could be dynamically displayed through the cascading "light trigger-heat generation-dynamic fluorescence output" conduction process (Figure 4F; Figure S25, Supporting Information).

**ADVANCED
SCIENCE NEWS**

www.advancedsciencenews.com
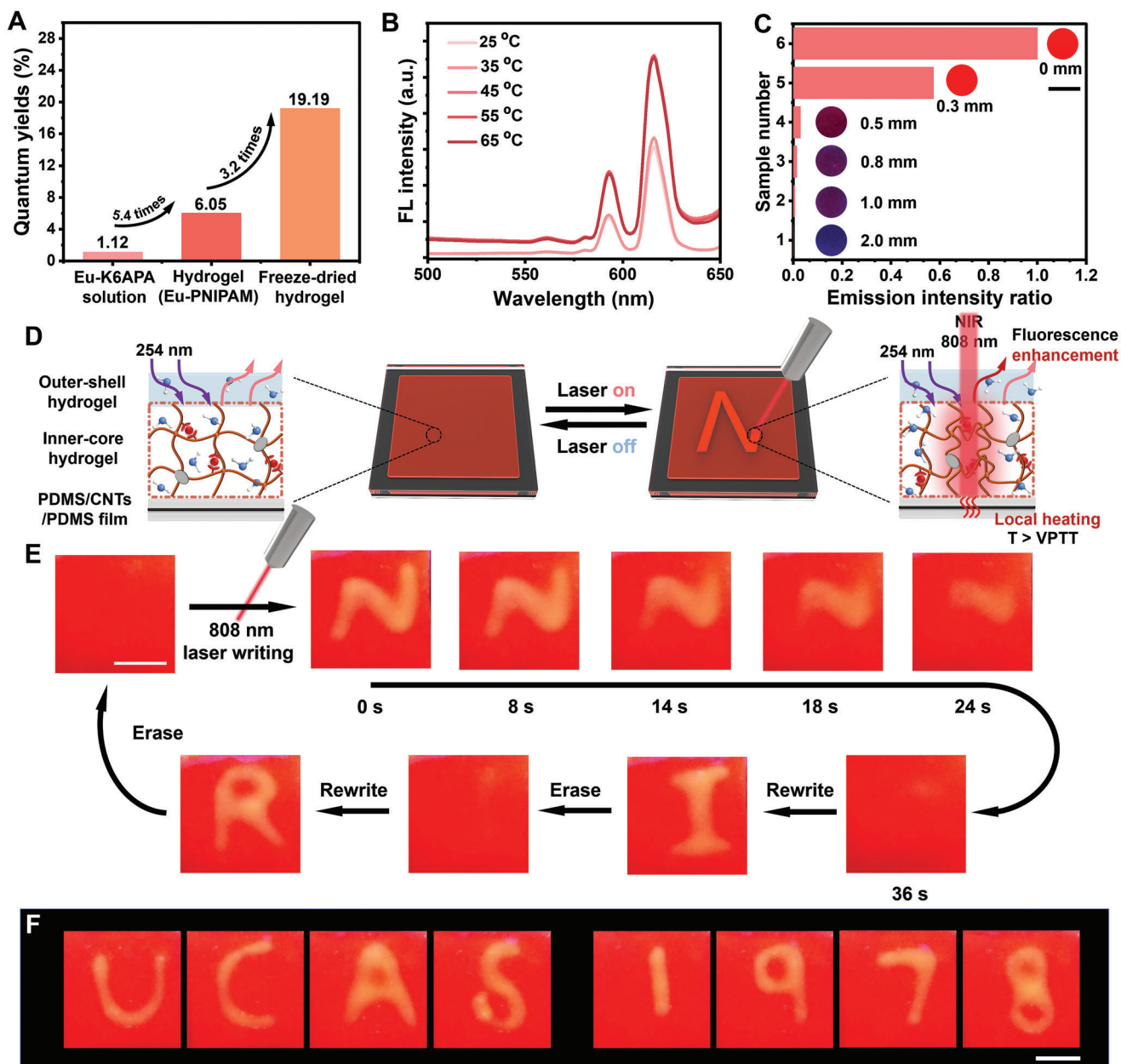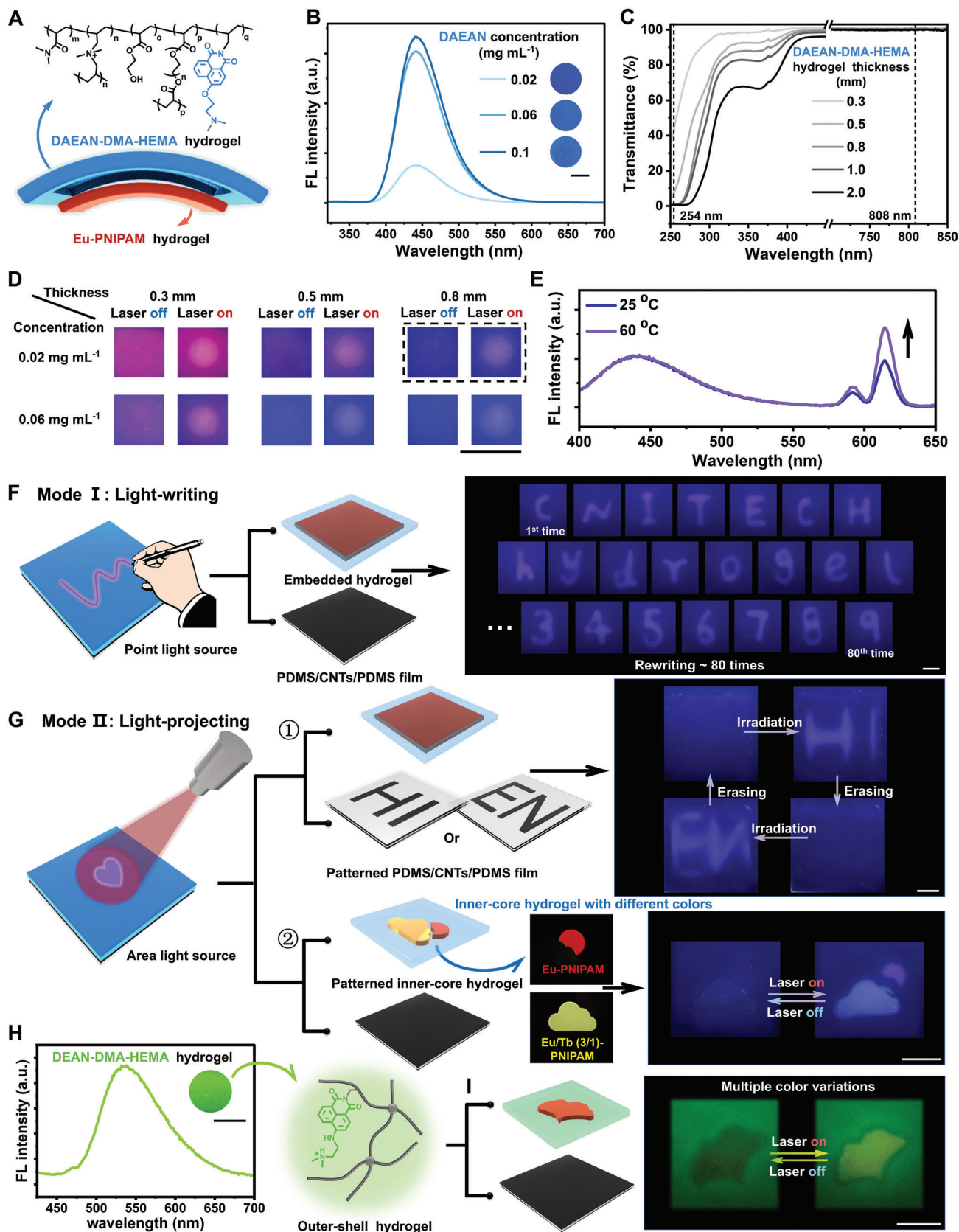
**ADVANCED
MATERIALS**

www.advmat.de

Figure 4. Studies on the "light trigger–heat generation–dynamic fluorescence output" cascading process of the rewritable hydrogel display system. A) Photoluminescence quantum yields of Eu-K6APA solution, Eu-PNIPAM hydrogel, and freeze-dried Eu-PNIPAM hydrogel. B) Fluorescence spectra (λ_{ex} = 254 nm) of the inner-core Eu-PNIPAM hydrogel at different temperature. C) The red emission intensity ratio (I_t/I_0) at 614 nm of the embedded hydrogels as a function of the outer-shell hydrogel thickness, as well as the corresponding fluorescent photographs. (I_t and I_0 denote the fluorescent intensity of embedded hydrogels with different-thickness outer-shell hydrogels and free Eu-PNIPAM hydrogel, respectively.) D) Schematic illustration showing the cascading display mechanism of "light trigger–heat generation–dynamic fluorescence output". E) Digital photos showing the NIR light-written "N" letter on the hydrogel display system that gradually self-erased after turning off the NIR laser to allow the rewriting of other letters such as "I" or "R". F) Fluorescent photos exhibiting various NIR light-written information like "UCAS", and "1978" on the hydrogel display system. Scale bars in digital photos are 1 cm. Photos were taken under a 254 nm UV lamp.

2.4. Light-Writing & Projecting Display of Multicolor Information

For the display of multicolor information to better visual information interactive experience, it is essential to realize NIR light triggered multicolor fluorescence changes of the hydrogel display layer. To this end, blue-light-emitting 4-(dimethylamino)ethoxy-

N-allyl-1,8-naphthalimide (DAEAN) monomer was covalently introduced into the outer-shell hydrogel matrix to construct the dual-emissive embedded hydrogel, whose emission color came from the spectral overlapping of inner-core Eu-PNIPAM and outer-shell DAEAN-DMA-HEMA hydrogel layers (**Figure 5**A). To achieve distinct NIR laser triggered fluorescence color response,

F Mode I: Light-writing

G Mode II: Light-projecting

H

**ADVANCED
SCIENCE NEWS**

www.advancedsciencenews.com

**ADVANCED
MATERIALS**

www.advmat.de

both material composition and geometry thickness of the outer-shell DAEAN-DMA-HEMA hydrogel were optimized. As presented in Figure 5B,C; Figure S26 (Supporting Information), it was found that its blue emission intensity rose with increasing DAEAN concentration, and the excitation UV light transmittance showed negative dependence on its thickness. For example, as shown in Figure 5D, when the DAEAN concentration and hydrogel thickness were relatively small (0.02 mg mL^{-1}, 0.3 mm), overlapping color of the embedded hydrogel was magenta at ambient conditions. Under NIR illumination, the red fluorescence of inner-core Eu-PNIPAM hydrogel was enhanced, resulting in magenta-to-pink color change. Subsequently, violet-to-magenta fluorescence color change was observed by either increasing the DAEAN concentration (0.06 mg mL^{-1}, 0.3 mm) or thickness (0.02 mg mL^{-1}, 0.5 mm). Further optimizing the DAEAN concentration as 0.02 mg mL^{-1} and outer-shell hydrogel thickness as 0.8 mm can achieve distinct blue-to-violet color transition under NIR laser stimulation. Such noticeable color change was consistent with the recorded fluorescence spectra of the whole system, which showed that the intensity of blue fluorescence band centered at 443 nm was almost constant when increasing the temperature from 25°C to 60°C, while the intensity of red fluorescence band centered at 614 nm was obviously enhanced (Figure 5E).

Having realized the NIR-light-induced blue-to-violet fluorescence color change, real-time handwriting display of transient information was further explored by utilizing the non-contact NIR light as a "pen". As shown in Figure 5F, the handwriting area was relatively small, because the NIR laser employed here was a point light source. Owing to the fast and reversible phase transition of the inner-core Eu-PNIPAM hydrogel, this light-writing mode was proved to be real-time and self-erasable, enabling the reversible display of arbitrary hand-written information. For example, dynamic information like "CNITECH", "hydrogel" and "3456789" (Uppercase letters, lowercase letters, and Arabic numerals) could be successively written on the same rewritable system. It should be emphasized that the hydrogel is only locally heated during the NIR light-writing display process, because the diameter of NIR light spot on the photothermal layer is usually well-controlled to within 2 mm for ensuring better information display. Also, each NIR light-writing and self-erasing cycle only lasts tens of seconds (<40 s), resulting in very little water evaporation. Therefore, the NIR light-induced "writing/self-erasing/rewriting" processes of our display system could be repeated for more than 80 times without affecting legibility and intactness of the written information (Figure 5F).

Besides the NIR light-writing mode that enabled real-time and transient handwriting display of arbitrary information, NIR light-projecting mode was further demonstrated to allow for the sustainable display of predesigned information by using an area light source. As schemed in Figure 5G, there were two ways to achieve the NIR light-projecting display. The first way was to use the pre-patterned photothermal CNTs film (Figure S27, Supporting Information). For example, when the CNTs film was pre-engineered to the "HI" pattern, the information "HI" would be rapidly displayed on the rewritable system upon exposure to NIR light source whose area is larger than the pattern. After removing the NIR laser, the "HI" pattern gradually disappeared. Importantly, the photothermal control layer that was supramolecularly bonded with the hydrogel display layer could be easily peeled by external force, suggesting the possibility for the photo-projecting display of new information (e.g., "EN") by simply replacing the photothermal CNTs film with a different pattern. The second way was to engineer the shape of inner-core hydrogel. Note that the emission color of lanthanide-coordinated inner-core hydrogels was able to be modulated from red to green by controlling the Eu^{3+}/Tb^{3+} molar ratio (Figure S28, Supporting Information). Therefore, yellow-light-emitting Eu/Tb-PNIPAM (Eu^{3+}/Tb^{3+} = 3:1) hydrogel as the "cloud" and red-light-emitting Eu-PNIPAM hydrogel as the "sun" were then embedded in the blue-light-emitting DAEAN-DMA-HEMA hydrogel. As shown in Figure 5G, no pattern information was noticed when the NIR laser was off. Once irradiated with the 808 nm area light source, one colorful image containing "blue sky", "white cloud", and "violet sun" was clearly displayed. Obviously, the multicolor fluorescence changes were capable of be employed to convey colorful figures or patterns, suggesting the significance of color diversification for multi-information display.

In addition, the NIR-light-triggered fluorescence color variation of our multicolor display systems can also be achieved by varying the material composition of outer-shell hydrogel. To demonstrate this potential, an outer-shell DEAN-DMA-HEMA hydrogel with green fluorescence was obtained by covalently introducing 4-(*N, N*-dimethylaminoethylene)amino-*N*-allyl-1,8 naphthalimide (DEAN) into hydrogel matrix (Figure 5H). When one red-light-emitting inner-core Eu-PNIPAM hydrogel with a ginkgo leaf pattern was embedded into this new outer-shell DEAN-DMA-HEMA hydrogel, NIR light-projecting reversible display of the ginkgo leaf from dark green to yellow was demonstrated upon power off-on of the area light source (Figure 5I). The design of this embedded multilayer structure provides a simple yet effective construction strategy for achieving multicolor

---

Figure 5. Light-writing and projecting display of multicolor information. A) Schematic illustration of the embedded hydrogel with dual emission, as well as the chemical structure of its outer-shell DAEAN-DMA-HEMA hydrogel. B) Fluorescence spectra (λ_{ex} = 254 nm) and digital photos of DAEAN-DMA-HEMA hydrogels with different DAEAN concentrations. C) Transmittance spectra of DAEAN-DMA-HEMA hydrogel with different thicknesses. D) Photos showing NIR light-responsive fluorescence color changes of hydrogel display systems with different material composition and geometry thickness. E) Thermo-responsive fluorescence spectra (λ_{ex} = 254 nm) of the embedded hydrogel sample with optimized DAEAN concentration as 0.02 mg mL^{-1} and outer-shell hydrogel thickness as 0.8 mm. F) Light-writing display of transient information such as English letters and Arabic numbers by using point light source. G) Light-projecting reversible display of predesigned multicolor patterns by using area light source. ① Light-projecting display of the "HI" pattern by pre-designed the CNTs film to the "HI" pattern, and then the "EN" pattern by pre-designed the CNTs film to the "EN" pattern. ② Light-projecting display of multicolor patterns by pre-designed the inner-core hydrogel to red fluorescent sun (Eu-PNIPAM) and yellow fluorescent cloud (Eu/Tb-PNIPAM with molar ratio of Eu^{3+}/Tb^{3+} as 3/1). H) Fluorescence spectra (λ_{ex} = 254 nm) and photo of the outer-shell DEAN-DMA-HEMA hydrogel. I) Light-projecting reversible display of the dark green and yellow ginkgo leaf by pre-designed the inner-core hydrogel to red fluorescent ginkgo leaf (Eu-PNIPAM) and the outer-shell hydrogel to green fluorescent DEAN-DMA-HEMA hydrogel. Scale bars in digital photos are 1 cm. All fluorescent photos were taken under a 254 nm UV lamp.

**ADVANCED
SCIENCE NEWS**

www.advancedsciencenews.com

**ADVANCED
MATERIALS**

www.advmat.de

variations of material patterns, further advancing the development of high-end products with better visual information interactive experience.

3. Conclusion

Inspired by the vertically arranged multilayer structure of different chromatophores that accounted for fast, reversible, and multicolor pattern display in chameleon skins, we developed a conceptually new type of flexible NIR-light-triggered rewritable multicolor hydrogel system for on-demand information display. The developed systems were specially engineered to have the bioinspired multilayer layout consisting of a fluorescent hydrogel layer as the display unit and an efficient PDMS-sealed photothermal stacked CNTs film layer as the control unit. Notably, the hydrogel layer was specially designed into an embedded structure where a thermo-responsive fluorescent hydrogel as inner core is constrained within a non-responsive outer-shell hydrogel to ensure the intact, reversible, and multicolor information loading. Under the non-contact remote irradiation of NIR light, the CNTs film rapidly completed photothermal conversion and instantly transferred the local heat to trigger distinct fluorescence color changes of the hydrogel display layer. Based on this well-established cascading process of "light trigger–heat generation–dynamic fluorescence output", arbitrary information (e.g., numbers, letters) could be instantly hand-written on our display systems within 5 s by using NIR light as a pen, and transiently self-erased for another rewriting cycle within 36 s. Remarkably, such NIR light-writing/self-erasing/rewriting cycles were proved to be repeated for at least 80 times without affecting legibility and intactness of the written information. Besides the light-writing display of transient information, the sustainable light-projecting display of predesigned multicolor patterns was also achieved because of the unique multilayer layout that facilitated easy patterning of the photothermal control layer or hydrogel display layer. Additionally, such multilayer embedded structure design of the hydrogel display unit also allowed the introduction of different-colored fluorophores into the inner-core and outer-shell hydrogels, further enriching the color diversification of information display to better visual information interactive experience. Furthermore, to better illustrate the characteristics of reversible photothermal writing, a comparison table (Table S1, Supporting Information) has been made, which summarizes the reported characteristics (response time, recovery time, number of color changes, and writing style) of our system and many representative light-writing systems reported in the literature.

The bioinspired multilayer structure design, which allows for both fast NIR-light-writing/self-erasing/rewriting display of arbitrary transient information and sustainable NIR-light-projecting display of predesigned multicolor patterns, is key point of the present systems, in contrast to the reported homogeneous rewritable display system. In view of its modular design principle, the proposed strategy is believed to be generally applicable. For instance, a wide variety of thermo-responsive soft materials with diverse structure/pigment color changes are potentially employed as the display layer. The control layer is also not limited to the CNTs film, as there exist a large number of high-efficiency photothermal materials, including graphene, MXenes, MoS_2, MOF, noble metals, polypyrrole, and so on.[16] Interest-

ingly, the hydrogel display layer and the photothermal control layer are bonded by supramolecular interaction, so they can be easily disassembled and reassembled to meet the various systems of different display units and control units. The display systems proposed herein are thus expected to inspire the future development of many novel NIR light-writing systems with expanded functionalities and wide potential applications for visual information display, encryption, transmission, etc.

4. Experimental Section

Materials: *N*-Isopropylacrylamide (NIPAM, 98.0%) was purchased from TCI (Shanghai) Development Co., Ltd. *N,N′*-Methylene bis(acrylamide) (MBAA, ≥98.0%), diallyldimethylammonium chloride (DADMAC, 60% in water), ammonium peroxodisulfate (APS, ≥98.0%), *N,N,N′,N′*-tetramethylethylenediamine (TEMED, 99.0%), 2-Hydroxyethyl methacrylate (HEMA, 99.0%), $Eu(NO_3)_3 \cdot 6H_2O$ (99.9%), $Tb(NO_3)_3 \cdot 5H_2O$ (99.9%) were provided by Aladdin Chemistry Co. Ltd. Potassium hydroxide (KOH, 95.0%) was obtained from Energy Chemical. *N,N*-Dimethylacrylamide (DMA, 98%) was supplied by Shanghai Macklin Biochemical Co., Ltd. Poly(ethylene glycol) diacrylate (PEGDA) with average M_n of 700 was from Sigma-Aldrich. The raw carbon nanotubes (CNTs) with a purity of over 90% were commercially purchased from Chengdu Organic Chemistry Co. Ltd. PDMS (500 μm) films and PDMS precursor solutions were from Xi'an Ruiya Organic Chemistry Co. Ltd. and Sylgard 184 (Dowcorning, US), respectively. Synthetic nanoclays (formula: $Mg_{5.34}Li_{0.66}Si_8O_{20}(OH)_4Na_{0.66} + Na_4P_2O_7$, trademark: Laponite XLS) was purchased from BYK Additives & Instruments, Co., Ltd. The ligand monomer of 6-acrylamidopicolinic acid (6APA), blue fluorescent monomer 4-(2-dimethylaminoethyloxy)-*N*-allyl-1,8-naphthalimide (DAEAN), and yellow-green fluorescent monomer 4-(*N,N*-dimethylaminoethylene)amino-*N*-allyl-1,8 naphthalimide (DEAN) were synthesized according to previously reported methods.[17]

Preparation of Thermoresponsive Inner-Core Hydrogel: The thermo-responsive fluorescent polymeric hydrogels were prepared by thermally initiated radical polymerization. Laponite XLS (41 mg) was dispersed in deionized water (4.66 mL). Whereafter, NIPAM (822 mg), 6APA (10 mg), KOH (2.92 mg), MBAA (4.11 mg), and APS (8.22 mg) were added and mixed thoroughly. After addition of TEMED (6.7 μL) that served as initiator accelerator, the mixture was then transferred into the self-made molds containing two quartz glass and 0.8 mm thick silicon plate, followed by free radical copolymerization at 4 °C for above 24 h. Afterward, the obtained hydrogel was immersed in Eu^{3+} aqueous solution (0.1 M) for 15 min to form lanthanide complexes. After removing the excess ions in deionized water for another 15 min, the Eu-PNIPAN hydrogel with red fluorescence was obtained, which was used as inner-core hydrogel. Similarly, using aqueous solution of Tb^{3+} or mixed solution of Eu^{3+} and Tb^{3+} (molar ratio of 3:1), green-light-emitting (Tb-PNIPAN) or yellow-light-emitting (Eu/Tb-PNIPAM) hydrogels were fabricated.

Fabrication of the Hydrogel Layer with Embedded Structure: The hydrogel layer with an embedded structure was prepared by two-step thermally initiated radical polymerization. The fabrication procedure was shown in Figure S2 (Supporting Information). The 1st polymerization was aimed to prepare inner-core hydrogels mentioned above. The inner-core hydrogels were cut into desired shapes and then immersed in 10 mg mL^{-1} APS solution for more than 5 min. The specific soaking time was dependent on the size of hydrogels. After removing the excess solution with absorbent paper, inner-core hydrogel was transferred to a homemade mold for use. It should be noted that the dimensions (length, width, and height) of the hollow-out in the center of the mold needed to be larger than the inner-core hydrogels. Prior to the polymerization of outer-shell hydrogel, the precursor solution was prepared. Typically, Laponite XLS (51.48 mg) was first adequately dispersed in 6 mL deionized water by magnetic stirring. Then HEMA (429 mg), DMA (2145 mg), DADMAC water solution (343.2 mg), PEGDA (5.15 mg, 0.2 wt.% to the total amount of HEMA and DMA), as

**ADVANCED
SCIENCE NEWS**

www.advancedsciencenews.com

**ADVANCED
MATERIALS**

www.advmat.de

well as APS (51.48 mg) were added to this nanoclay solution and mixed completely. After introducing TEMED (70.5 µL), the as-prepared precursor solution was poured into the homemade mold that contained the inner-core hydrogel. The 2nd polymerization was conducted at 4 °C for 1.0 h. After de-molding, the embedded hydrogel was obtained. Additionally, to produce the embedded hydrogel with blue fluorescent outer-shell, the organic DAEAN fluorophore was introduced in the precursor solution of outer-shell hydrogel. Other steps remained the same. By this method, outer-shell hydrogels with different concentrations of DAEAN (0.02, 0.06, 0.1 mg mL^{-1}) can be constructed. Similar procedures were used for fabricating pure outer-shell hydrogels without embedded structure. The outer-shell hydrogels with or without DAEAN were named DAEAN-DMA-HEMA and DMA-HEMA hydrogel, respectively. Similarly, DEAN-DMA-HEMA hydrogel with 0.25 mg mL^{-1} DEAN was constructed.

Fabrication of PDMS/CNTs/PDMS Film: The condensed CNTs film at the air/water interface was fabricated according to the Langmuir-Blodgett method reported in previous work.[11] Specifically, anhydrous ethanol was used as dispersant to form uniform CNTs suspensions (0.5 mg mL^{-1}). Subsequently, a certain volume of the as-prepared dispersion was spread onto the water surface at a certain angle, distance, and speed to form a stable ultrathin CNTs film. Next, a porous sponge was selected to gradually insert into one side of the interface, and the preassembled film was squeezed controllably by the generated capillary force to obtain a densely stacked CNTs film. The compression procedure was repeated until the area of the CNTs film no longer changed. Then using the lift-up transferring method, the condensed CNTs film floating on air/water interface was transferred to commercial PDMS film with thickness of 0.5 mm, followed by a drying procedure at 60 °C to obtain one-layered CNTs/PDMS film. A sequence of CNTs/PDMS with different ply numbers of condensed CNTs films (0 ≈ 4) can be prepared just by repeating the transferring and drying processes. Finally, the dried CNTs/PDMS film was placed into a 1.0 mm thick silicon plate. Then, the PDMS precursor solution with the weight ratio of base agent to curing agent 10:1 was added on the CNTs side of CNTs/PDMS film and scraped evenly by a plastic blade. After curing at 60 °C for 2 h, PDMS/CNTs/PDMS-x films with sandwiched structure were fabricated.

Light-Writing and Projecting Modes of Photothermally Controlled Rewritable Hydrogel Display System: The embedded hydrogel was hand-pressed to supramolecularly adhered to the PDMS/CNTs/PDMS-3 film for constructing the photothermally controlled rewritable hydrogel display system with a multilayer structure. For light-writing mode, both the CNTs film and inner-core hydrogel had a regular rectangular plane without any pattern. For light-projecting modes, either the patterned CNTs film or patterned hydrogel layer was used. The patterned CNTs film was fabricated using a thick silicon plate as the mask in the transferring process, while the patterned inner-core hydrogel was made by a laser cutting machine.

Characterization: Morphologies of the samples were characterized using polarizing microscope (OLYMPUS BX51) and field-emission scanning electron microscopy (SEM, Hitachi S-4800). The FT-IR spectra were measured by micro-FTIR (Agilent Cary660+620). XPS characterization was obtained from Kratos AXIS SUPRA instrument with a monochromic Al Kα X-ray source. The UV-vis absorption and optical transmittance spectra were recorded on PerkinElmer LAMBDA 950 UV/Vis/NIR spectrophotometer. Zwick Z1.0 universal testing machine equipped with a 1 KN load cell was used to test the tensile mechanical performances of the hydrogels with 100 mm min^{-1} and lap shear adhesion between outer-shell hydrogel and PDMS with 50 mm min^{-1}. DSC experiments were performed with a differential scanning calorimeter (Netzsch DSC-214) under nitrogen atmosphere with a heating rate of 1.5 °C min^{-1}. Dynamic rheological measurements of hydrogels with 25 mm parallel plates were conducted with a stress-controlled rheometer (HR-3, TA) on a temperature sweep (4 °C min^{-1}) at a constant angular frequency of 1 rad s^{-1} and shear strain of 0.2%. NIR light was provided by an NIR laser source (K808DAHFN-15.00 W, 808 nm, BWT Beijing). The real-time surface temperature and IR thermal images of the samples were monitored by IR thermal camera (Optris PI 400). The fluorescent images of samples were recorded by smart phone camera under a UV lamp (UVL-28, 8 W, 254 nm). A Horiba FL3-111 fluorescence spectrofluorometer was used to measure the steady-state fluorescence spectra of hydrogels. The photoluminescence quantum yields (λ_{ex} = 254 nm) were measured by quantum efficiency tester (Otsuka Photal Electronics QE-2100).

Supporting Information

Supporting Information is available from the Wiley Online Library or from the author.

Acknowledgements

Conflict of Interest

The authors declare no conflict of interest.

Data Availability Statement

Research data are not shared.

Keywords

[1] a) M. I. Khazi, W. Jeong, J. M. Kim, *Adv. Mater.* **2018**, *30*, 1705310; b) R. Chen, Y. Yu, S. Xie, H. Zhao, S. Liu, J. Ren, H.-Z. Tan, *Sustainability* **2020**, *12*, 7192.

[2] a) L. Mao, Z. Wang, Y. Duan, C. Xiong, C. He, X. Deng, Y. Zheng, D. Wang, *ACS Nano* **2021**, *15*, 10384; b) R. Chen, D. Feng, G. Chen, X. Chen, W. Hong, *Adv. Funct. Mater.* **2021**, *31*, 2009916; c) Y. Ma, Y. Yu, P. She, J. Lu, S. Liu, W. Huang, Q. Zhao, *Sci. Adv.* **2020**, *6*, eaaz2386; d) J. Deng, H. Wu, W. Xie, H. Jia, Z. Xia, H. Wang, *ACS Appl. Mater. Interfaces* **2021**, *13*, 39967; e) W. Li, M. Yin, J. Liu, H. Fu, X. Shao, Y. Dong, Q. Song, C. Zhang, W. Y. Wong, *Mater. Horiz.* **2022**, *9*, 2198; f) Q. Wang, Z. Qi, Q. M. Wang, M. Chen, B. Lin, D. H. Qu, *Adv. Funct. Mater.* **2022**, *32*, 2208865; g) P. She, Y. Ma, Y. Qin, M. Xie, F. Li, S. Liu, W. Huang, Q. Zhao, *Matter* **2019**, *1*, 1644; h) Q. Wang, Q. Zhang, Q. W. Zhang, X. Li, C. X. Zhao, T. Y. Xu, D. H. Qu, H. Tian, *Nat. Commun.* **2020**, *11*, 158; i) X. Le, H. Shang, H. Yan, J. Zhang, W. Lu, M. Liu, L. Wang, G. Lu, Q. Xue, T. Chen, *Angew. Chem., Int. Ed.* **2021**, *60*, 3640; j) Z. Gao, S. Qiu, F. Yan, S. Zhang, F. Wang, W. Tian, *Chem. Sci.* **2021**, *12*, 10041; k) Z. Wang, D. Xie, F. Zhang, J. Yu, X. Chen, C. P. Wong, *Sci. Adv.* **2020**, *6*, eabc2181.

**ADVANCED
SCIENCE NEWS**

www.advancedsciencenews.com

**ADVANCED
MATERIALS**

www.advmat.de

[3] a) L. Qin, W. Gu, J. Wei, Y. Yu, *Adv. Mater.* **2018**, *30*, 1704941; b) L. Li, J. M. Scheiger, P. A. Levkin, *Adv. Mater.* **2019**, *31*, 1807333.

[4] a) Z. Li, X. Liu, G. Wang, B. Li, H. Chen, H. Li, Y. Zhao, *Nat. Commun.* **2021**, *12*, 1363; b) J. Zhang, H. Shen, X. Liu, X. Yang, S. L. Broman, H. Wang, Q. Li, J. W. Y. Lam, H. Zhang, M. Cacciarini, M. B. Nielsen, B. Z. Tang, *Angew. Chem., Int. Ed.* **2022**, *61*, 202208460; c) J. Li, H. Bisoyi, S. Lin, J. Guo, Q. Li, *Angew. Chem., Int. Ed.* **2019**, *58*, 16052; d) Y. Ma, J. Shen, J. Zhao, J. Li, S. Liu, C. Liu, J. Wei, S. Liu, Q. Zhao, *Angew. Chem., Int. Ed.* **2022**, *61*, 202202655; e) H. Wu, Y. Chen, Y. Liu, *Adv. Mater.* **2017**, *29*, 1605271; f) V. Muller, T. Hungerland, M. Baljozovic, T. Jung, N. D. Spencer, H. Eghlidi, P. Payamyar, A. D. Schluter, *Adv. Mater.* **2017**, *29*, 1701220; g) D. Okada, Z.-H. Lin, J.-S. Huang, O. Oki, M. Morimoto, X. Liu, T. Minari, S. Ishii, T. Nagao, M. Irie, Y. Yamamoto, *Mater. Horiz.* **2020**, *7*, 1801; h) W. Wang, N. Xie, L. He, Y. Yin, *Nat. Commun.* **2014**, *5*, 5459; i) Z. Zhang, W. Wang, P. Jin, J. Xue, L. Sun, J. Huang, J. Zhang, H. Tian, *Nat. Commun.* **2019**, *10*, 4232; j) Y. Niu, S. Li, J. Zhang, W. Wan, Z. He, J. Liu, K. Liu, S. Ren, L. Ge, X. Du, Z. Gu, *Small* **2021**, *17*, 2102224.

[5] a) W. C. Xu, C. Liu, S. Liang, D. Zhang, Y. Liu, S. Wu, *Adv. Mater.* **2022**, *34*, 2202150; b) Y. Liu, S. Liang, C. Yuan, A. Best, M. Kappl, K. Koynov, H. J. Butt, S. Wu, *Adv. Funct. Mater.* **2021**, *31*, 2103908; c) J. Liu, Y. Wang, J. Wang, G. Zhou, T. Ikeda, L. Jiang, *ACS Appl. Mater. Interfaces* **2021**, *13*, 12383.

[6] a) X. Le, H. Shang, S. Wu, J. Zhang, M. Liu, Y. Zheng, T. Chen, *Adv. Funct. Mater.* **2021**, *31*, 2108365; b) W. Miao, S. Wang, M. Liu, *Adv. Funct. Mater.* **2017**, *27*, 1701368; c) T. Zhang, L. Sheng, J. Liu, L. Ju, J. Li, Z. Du, W. Zhang, M. Li, S. X.-A. Zhang, *Adv. Funct. Mater.* **2018**, *28*, 1705532.

[7] Y. Wang, Q. Zhao, X. Du, *Mater. Horiz.* **2020**, *7*, 1341.

[8] J. Liu, Q. Guo, X. Zhang, J. Gai, C. Zhang, *Adv. Funct. Mater.* **2021**, *31*, 2106673.

[9] a) J. Teyssier, S. V. Saenko, D. van der Marel, M. C. Milinkovitch, *Nat. Commun.* **2015**, *6*, 6368; b) G. Isapour, M. Lattuada, *Adv. Mater.* **2018**, *30*, 1707069; c) W. Lu, M. Si, X. Le, T. Chen, *Acc. Chem. Res.* **2022**, *55*, 2291.

[10] a) M. Hua, S. Wu, Y. Ma, Y. Zhao, Z. Chen, I. Frenkel, J. Strzalka, H. Zhou, X. Zhu, X. He, *Nature* **2021**, *590*, 594; b) M. Qin, M. Sun, R. Bai, Y. Mao, X. Qian, D. Sikka, Y. Zhao, H. J. Qi, Z. Suo, X. He, *Adv. Mater.* **2018**, *30*, 1800468; c) L. Zhang, H. Yan, J. Zhou, Z. Zhao, J. Huang, L. Chen, Y. Ru, M. Liu, *Adv. Mater.* **2023**, 2202193; d) G. Nian, J. Kim, X. Bao, Z. Suo, *Adv. Mater.* **2022**, *34*, 2206577; e) Y. W. Lee, S. Chun, D. Son, X. Hu, M. Schneider, M. Sitti, *Adv. Mater.* **2022**, *34*, 2109325; f) L. Hu, Q. Zhang, X. Li, M. J. Serpe, *Mater. Horiz.* **2019**, *6*, 1774; g) Q. Zhang, Y. Zhang, Y. Wan, W. Carvalho, L. Hu, M. J. Serpe, *Prog. Polym. Sci.* **2021**, *116*, 101386; h) C. N. Zhu, C. Y. Li, H. Wang, W. Hong, F. Huang, Q. Zheng, Z. L. Wu, *Adv. Mater.* **2021**, *33*, 2008057; i) C. N. Zhu, T. Bai, H. Wang, J. Ling, F. Huang, W. Hong, Q. Zheng, Z. L. Wu, *Adv. Mater.* **2021**, *33*, 2102023; j) L. Tang, L. Wang, X. Yang, Y. Feng, Y. Li, W. Feng, *Prog. Mater. Sci.* **2020**, *115*, 100702; k) Z. Li, X. Ji, H. Xie, B. Z. Tang, *Adv. Mater.* **2021**, *33*, 2100021; l) Y. Yang, Q. Li, H. Zhang, H. Liu, X. Ji, B. Z. Tang, *Adv. Mater.* **2021**, *33*, 2105418; m) D. Hao, Z. Wang, M. Liu, X. Guo, S. Wang, L. Jiang, *Angew. Chem., Int. Ed.* **2023**, *62*, 202215034; n) J. Liu, S. Lin, X. Liu, Z. Qin, Y. Yang, J. Zang, X. Zhao, *Nat. Commun.* **2020**, *11*, 1017.

[11] a) J. Zhu, M. Yao, S. Huang, J. Tian, Z. Niu, *Angew. Chem., Int. Ed.* **2020**, *59*, 16480; b) X. Xu, S. Ozden, N. Bizmark, C. B. Arnold, S. S. Datta, R. D. Priestley, *Adv. Mater.* **2021**, *33*, 2007833.

[12] B. Sun, Y. Lin, P. Wu, H. W. Siesler, *Macromolecules* **2008**, *41*, 1512.

[13] a) S. Wei, H. Qiu, H. Shi, W. Lu, H. Liu, H. Yan, D. Zhang, J. Zhang, P. Theato, Y. Wei, T. Chen, *ACS Nano* **2021**, *15*, 10415; b) H. Shi, S. Wu, M. Si, S. Wei, G. Lin, H. Liu, W. Xie, W. Lu, T. Chen, *Adv. Mater.* **2022**, *34*, 2107452.

[14] a) G. Weng, S. Thanneeru, J. He, *Adv. Mater.* **2018**, *30*, 1706526; b) K. Meng, C. Yao, Q. Ma, Z. Xue, Y. Du, W. Liu, D. Yang, *Adv. Sci.* **2019**, *6*, 1802112.

[15] a) S. V. Eliseeva, J. C. Bunzli, *Chem. Soc. Rev.* **2010**, *39*, 189; b) P. Kumar, S. Soumya, E. Prasad, *ACS Appl. Mater. Interfaces* **2016**, *8*, 8068.

[16] a) X. Sun, C. Huang, L. Wang, L. Liang, Y. Cheng, W. Fei, Y. Li, *Adv. Mater.* **2021**, *33*, 2001105; b) Q. Zheng, X. Liu, Y. Zheng, K. W. K. Yeung, Z. Cui, Y. Liang, Z. Li, S. Zhu, X. Wang, S. Wu, *Chem. Soc. Rev.* **2021**, *50*, 5086.

[17] a) S. Wei, W. Lu, X. Le, C. Ma, H. Lin, B. Wu, J. Zhang, P. Theato, T. Chen, *Angew. Chem., Int. Ed.* **2019**, *58*, 16243; b) H. Qiu, S. Wei, H. Liu, B. Zhan, H. Yan, W. Lu, J. Zhang, S. Wu, T. Chen, *Adv. Intell. Sys.* **2021**, *3*, 2000239; c) P. Li, D. Zhang, Y. Zhang, W. Lu, J. Zhang, W. Wang, Q. He, P. Théato, T. Chen, *ACS Macro Lett.* **2019**, *8*, 937.